COVER SHEET

Raman spectroscopy of uranopilite of different origin - implications for molecular structure

Ray L. Frost [a•], Jiří Čejka [b], Matt L. Weier [a], Wayde N. Martens [a] and Godwin A. Ayoko [a]

[a] Inorganic Materials Research Program, School of Physical and Chemical Sciences, Queensland University of Technology, GPO Box 2434, Brisbane Queensland 4001, Australia.

[b] National Museum, Václavské náměstí 68, CZ-115 79 Praha 1, Czech Republic.

Abstract

Uranopilite, $[(UO_2)_6(SO_4)O_2(OH)_6(H_2O)_6](H_2O)_8$, the composition of which may vary, can be understood as a complex hydrated uranyl oxy hydroxy sulfate. The structure of uranopilite of different localities has been studied by Raman spectroscopy at 298 and 77 K. A single intense band at 1009 cm^{-1} assigned to the ν_1 $(SO_4)^{2-}$ symmetric stretching mode shifts to higher wavenumbers at 77 K. Three low intensity bands are observed at 1143, 1117 and 1097 cm^{-1}. These bands are attributed to the $(SO_4)^{2-}$ ν_3 antisymmetric stretching modes. Multiple bands provide evidence that the symmetry of the sulphate anion in the uranopilite structure is lowered. Three bands are observed at 843 to 816 cm^{-1} in both 298 and 77 K spectra and are attributed to the ν_1 symmetric stretching modes of the $(UO_2)^{2+}$ units. Multiple bands prove the symmetry reduction of the UO_2 ion. Multiple OH stretching modes prove a complex arrangement of OH groupings and hydrogen bonding in the crystal structure. A series of infrared bands not observed in the Raman spectra are found at 1559, 1540, 1526 and 1511 cm^{-1} attributed to δ UOH bending modes. U-O bond lengths in uranyl and O-H…O bond lengths are calculated and compared with X-ray single crystal structure analysis. Raman spectra of uranopilites of different origin show subtle differences in spectra proving the spectra are origin and sample dependent. Hydrogen-bonding network and its arrangement in the crystal structure play an important role in the origin and stability of uranopilite.

Keywords: uranopilite, johannite, zippeite, uranyl sulphate minerals, dehydroxylation, dehydration, infrared and Raman spectroscopy

---

• Author to whom correspondence should be addressed (r.frost@qut.edu.au)

Introduction

The proposal to use nuclear power for the generation of electricity in China and the use of nuclear energy for desalination in Australia implies that there will be an increased mining of uranium minerals. Thus the mine waste from these mines such as at Ranger Mine in Northern territory, Australia, Olympic Dam and Beverley in South Australia implies increased environmental hazards. The realisation of the mobility of actinide compounds is of increasing importance both scientifically and socially. This is particularly so when uranium deposits are located in sensitive environmental areas such as adjacent to national parks for example Kakadu National Park in Australia. The Ranger mine and associated town of Jabiru is about 230 kilometres east of Darwin, surrounded by the Kakadu National Park, a major tourist attraction. The Olympic Dam copper and uranium mine, with the town of Roxby Downs, is located 560 km north of Adelaide, near the opal mining centre of Andamooka. This is an arid part of Australia, receiving only an average of only 160 mm of rain per year, and that rather unreliably. The massive deposit is underground, some 350 metres below the surface, and is the largest known uranium orebody in the world. It is most likely that due to the presence of sulphide ore bodies that uranyl sulphates will be formed. Such minerals show significant solubility. Uranyl sulphate solid state and solution chemistry plays one of the most important roles in the actinide chemistry, mineralogy, geochemistry and "environmental chemistry" with regard to uranium(VI) migration in natural waters. Sulphate formation is also significant in the treatment of spent nuclear fuels. The formation of uranyl sulfate minerals can result from the oxidation of sulfide ores and the formation of acid sulfate soils. [1,2] These acid sulfate enriched soils can result in the increased mobility of uranium from uranium mineral deposits and radioactive waste repositories. Actinide sulfate complexes inclusive those of uranium are to be reflected in migration from a nuclear waste repository or in accidental site contamination. To gain an understanding of the geochemical behavior of such materials, fundamental knowledge of actinide sulfate chemistry and mineralogy is needed.

The chemistry of uranyl sulphate minerals has been undertaken over an extended period of time [3-6] Nováček [5,7] assumes that uranopilite, having the general formula $6UO_3.SO_3.xH_2O$ (x = 16 or 17), contains 16 or 17 H_2O. Frondel [8]writes that the best formula for uranopilite is $(UO_2)_6(SO_4)(OH)_{10}.12\ H_2O$. It is noted that in all these given examples the U/S ratio is 6/1. Nováček [7,9] described a natural phase which he calls β-uranopilite, $(UO_2)_6(SO_4)(OH)_{10}.5H_2O$, later named meta-uranopilite by Frondel [8]. Nováček [7,9] assumed that this natural phase may be a product of partial dehydration of uranopilite. However, it was proved [10,11] that a phase corresponding to meta-uranopilite is not formed by dehydration of uranopilite. Uranopilite dehydration and dehydroxylation processes partly overlap and are connected with the formation of X-ray amorphous phases. Partly dehydrated uranopilite, the composition of which corresponds to meta-uranopilite, is also X-ray amorphous. Thus, meta-uranopilite has remained as one of the insufficiently described uranyl minerals. [6] Some new not yet approved and published in detail hydrated uranyl oxy hydroxy sulphate minerals have been also mentioned [12-16]. Recently Burns [Burns 2001]. published a crystal structure for uranopilite and showed the formula to be $[(UO_2)_6(SO_4)O_2(OH)_6(H_2O)_6](H_2O)_8$. The mineral is of space group P_1 and consists of six distinct U^{6+} cations forming part of a uranyl $(UO_2)^{2+}$ chain. Burns states that

the uranyl ions are each coordinated by five ligands arranged at the equatorial vertices of pentagonal dipyramids and uranyl sulphate chains are linked to form the extended structure by hydrogen bonds bridging directly between the chains and to interstitial H_2O groups.

Some general comments are necessary to the origin of the same mineral species at the same and/or various localities. Uranyl minerals exhibit considerable structural and chemical diversity, and reflect geochemical conditions dominant during their formation. [17,18] It is obvious that the conditions of mineral origin in nature cannot be identical with those in a laboratory and in some cases probably neither comparable. Minerals usually originate at different localities under different conditions. Crystal structures of thus formed minerals may vary. Synthetic analogues of natural phases, i. e. of minerals, are synthesized under laboratory conditions which are mostly different from those in nature. Crystal structure of synthetic phases may be identical but also may differ from natural phases. In the case of hydrated minerals, in phases formed under different conditions (various localities, different laboratories and procedures) the hydrogen-bonding network may significantly vary. Because of the important role of water molecules in the crystal structures of minerals, the crystal structures of minerals may therefore also vary. These general conclusions are supported by published papers by Hawthorne. [19-21] Most uranyl phases are based on sheet or chain structures and usually contains several molecular water groups; thus, site-mixing, vacancies, as well as disorder in the orientation of hydrogen bonds and the polar water molecules may occur. An examination of the crystal; chemistry of molecular water in uranyl phases suggests that considerable residual entropy may be caused by disorder of hydrogen bonds associated with interstitial water groups. Differences in hydrogen-bonding network arrangement in e.g. uranopilite-type minerals need not be depicted via their X-ray powder patterns. Burns states that as is the case for most uranyl minerals, hydrogen bonding is of fundamental importance to the stability of the structure of uranopilite.

In the series uranopilite – schoepite were described natural phases containing sulfate anions in their structure: uranopilite, (insufficiently described meta-uranopilite) [7,9], jáchymovite [22], insufficiently described $(UO_2)_6(SO_4)_{0.1}O_2(OH)_{7.8}.$ nH_2O, $(UO_2)_6(SO_4)_{0.6}O_2(OH)_{6.8}.$ nH_2O, $(UO_2)_6(SO_4)_{0.7}O_2(OH)_{6.6}.$ nH_2O [13], schoepite, metaschoepite, dehydrated schoepite [23-25]. Hydrated uranyl oxy hydroxy sulfates in the series uranopilite-schoepite are products of hydrolytical precipitation from $(UO_2)^{2+}$ and $(SO_4)^{2-}$ containing solutions originating during hydration-oxidation weathering – alteration of primary U^{4+} containing minerals such as uraninite. [Meisser - written personal communication to J.Č.]. It may be assumed that end member of this hydrolysis is schoepite which forms when all $(SO_4)^{2-}$ ions are eliminated from the solid phase. As may be inferred from the formula of uranopilite, this mineral contains relatively large amounts of water molecules and hydroxyl ions. As mentioned above, chain structure is characteristic of uranopilite. Burns writes that *the chain of uranopilite found is the most complex chain found to date in a uranyl mineral. The chain is composed of uranyl pentagonal dipyramids linked by sharing equatorial edges to form six-membered clusters. Within these clusters, two oxygen atoms are bonded to three* $(UO_2)^{2+}$ *ions, and but all four of the equatorial anions that terminate the cluster are water molecules. Identical clusters of six dipyramids are linked by sharing vertices with* $(SO_4)^{2-}$ *tetrahedra, such that each tetrahedron is four-connected. Chains are linked into the three-dimensional structure by hydrogen bonds, both*

directly between adjacent chains, and to interstitial water molecules. Hydrogen bonds also extend between clusters of dipyramids within the same chain. It is evident from the uranopilite crystal structure and hydration degree, that any changes of conditions of uranopilite formation including those concerning hydrogen-bonding network may influence the crystal structure of uranopilite. This may be proved e.g. by infrared and Raman spectroscopy but such structural changes need not be inferred from the X-ray powder pattern because the phase are amorphous.

The infrared spectroscopy of uranyl sulphate compounds has been undertaken. [26] Raman spectroscopy has also been recently used to understand the chemistry of uranyl sulphates. [27] The spectroscopy has been based on treating the components of uranopilite as separate vibrating entities. [28,29] Thus the infrared spectra are assigned to $(UO_2)^{2+}$, $(SO_4)^{2-}$, $(OH)^-$ and H_2O units. Whether such as assumption is valid is questionable. One of the difficulties of studying the uranyl minerals is the potential overlap of bands from these different units. Both the ν_1 and ν_3 $(SO_4)^{2-}$stretching modes may overlap with UOH deformation modes. Čejka et al. have shown that a band at 930 cm^{-1} is assignable to the antisymmetric stretching modes of the $(UO_2)^{2+}$ units. The band appears to be very variable in position for zippeites. [30] Bands were identified at between 880 and 924 cm^{-1}. This may be caused and/or influenced by compositional changes and hydrogen-bonding network arrangements in natural and synthetic phases studied. The intensity of the ν_1 symmetric stretching vibration was very weak in the infrared spectrum of uranopilite and the band at 840 cm^{-1} was assigned to this vibration. Čejka reported the ν_3 antisymmetric stretching vibrations of the $(SO_4)^{2-}$ units at 1139 and 1118 cm^{-1} for one uranopilite sample and nine absorptions in the 1191 to 1067 cm^{-1} range for a second uranopilite sample. [30] Infrared absorption bands at 637 and 602 cm^{-1} were ascribed to the ν_4 $(SO_4)^{2-}$ bending modes. [30] The results of the infrared spectra as published by Čejka suggest a sample dependence of the vibrational modes of uranopilite and uncertainty exists in the actual position of the bands. [30] Thus further research is required to understand the chemistry of uranopilite. The role of the arrangement of hydrogen bonds in the crystal structures of uranopilite samples of various localities should be therefore respected. The Raman spectrum of uranopilite was presented by Frost et al. [31-33]. It is known that the spectra of uranyl sulfate minerals may be also influenced by sample preparation as is the case of johannite. [30,34] Changes in the hydrogen-bonding network play an important role in these cases.

It is probable that some variation in chemical composition of uranopilite can occur. [13,35] In this case the ratio of U/S is not 6/1 but something more i.e. U_6/S_x where x is <1. In these cases a formula of $[(UO_2)_{6.0}\ (SO_4)_x\ O_2\ (OH)_{8-2x}].n\ H_2O$ applies where x<1. The lack of sulphate is compensated by an increase in the [OH] units. Examples where x is 0.1, 0.6 and 0.6 are known. [13] Even though uranopilite may have variable compositions, Raman spectroscopy can provide understanding of the molecular structure of uranopilite. As part of our on-going research into the use of Raman spectroscopy to assist in the elucidation of the structure of minerals especially secondary minerals, we report the Raman spectra of uranopilite mineral samples from different origins. These Raman spectra are then related to the mineral structure.

Experimental

Minerals

The uranopilite minerals used in this work were obtained from Museum Victoria and Mineral research Company and originated from (a) Ranger No. 1 deposit, Jabiru, NT (b) South Alligator River, NT (c) Apex Mine, Lander Co., Nevada (d) Midnite Mine, Stevens Co., Washington.

Theoretical $(UO_2)^{2+}/(SO_4)^{2-}$ ratio in uranopilite is 6/1, while in the studied uranopilite samples is approximately 6/0.5 and somewhat varies. X-ray powder patterns of the studied samples are close to those of uranopilite with the exception of the sample from Midnite Mine. Its X-ray powder pattern may be better related to that of schoepite. However, the sample contains practically the same amounts of sulfate ions as was observed in the other three uranopilite samples. This supports an idea, that solid-solutions between uranopilite and schoepite with limited solubility may exist. Some variations may exist also in the water content. This causes problems in defining the formula because of spontaneous partial dehydration of uranopilite under normal conditions, i.e. temperature and pressure.

Raman spectroscopy

The crystals of uranopilite were placed on the stage of an Olympus BHSM microscope, equipped with 10x and 50x objectives and part of a Renishaw 1000 Raman microscope system, which also includes a monochromator, a filter system and a Charge Coupled Device (CCD). Raman spectra were excited by a HeNe laser (633 nm) at a resolution of 2 cm^{-1} in the range between 100 and 4000 cm^{-1}. Repeated acquisition using the highest magnification was accumulated to improve the signal to noise ratio. Spectra were calibrated using the 520.5 cm^{-1} line of a silicon wafer. In order to ensure that the correct spectra are obtained, the incident excitation radiation was scrambled. Previous studies by the authors provide more details of the experimental technique. Spectra at liquid nitrogen temperature were obtained using a Linkam thermal stage (Scientific Instruments Ltd, Waterfield, Surrey, England). Details of the technique have been published by the authors [36-39].

Infrared Spectroscopy

Infrared spectra were obtained using a Nicolet Nexus 870 FTIR spectrometer with a smart endurance single bounce diamond ATR cell. Spectra over the 4000–525 cm^{-1} range were obtained by the co-addition of 64 scans with a resolution of 4 cm^{-1} and a mirror velocity of 0.6329 cm/s. Spectral manipulation such as baseline adjustment, smoothing and normalisation was performed using the GRAMS® software package (Galactic Industries Corporation, Salem, NH, USA).

Spectroscopic manipulation such as baseline adjustment, smoothing and normalisation were performed using the Spectracalc software package GRAMS (Galactic Industries Corporation, NH, USA). Band component analysis was undertaken using the Jandel 'Peakfit' software package, which enabled the type of fitting, function to be selected and allows specific parameters to be fixed or varied accordingly. Band fitting was done using a Lorentz-Gauss cross-product function with the minimum number of component bands used for the fitting process. The Lorentz-Gauss ratio was maintained at values greater than 0.7 and fitting was undertaken until

reproducible results were obtained with squared correlations of r^2 greater than 0.995.

Results and Discussion

Background

The lowering of the $D_{\infty h}$ symmetry of the free uranyl, UO_2^{2+}, and Td symmetry of the SO_4^{2-} groups causes infrared and Raman activation of all UO_2^{2+} and SO_4^{2-} vibrations and splitting of doubly and triply degenerate vibrations in the spectra of uranopilite. Six symmetrically distinct uranyl groups and only one symmetrically distinct sulfate group are present in the crystal structure of uranopilite [15]. According to Hawthorne [19-21] from the general point of view, and the conclusions by Burns [15] concerning uranopilite, hydrogen bonding is of fundamental importance to the stability of the structure of uranopilite. Burns also proposed hydrogen bonding network in the crystal structure of uranopilite on the basis of crystal, chemical and bond-valence arguments. The assignment of the bands observed is therefore made with regard to all these assumptions. Even though uranopilite may be of a variable stoichiometry with the ratio of U/S varying according to the origin of the mineral sample. Raman spectroscopy will still measure the vibrational spectrum. Variation in intensity of the bands due to the vibrations of UO_2^{2+}, SO_4^{2-}, H_2O and OH units will occur according to this stoichiometry.

Raman spectroscopy

The Raman spectra of uranopilite at 298 and 77 K in the 750 to 1050 cm^{-1} region are shown in Figures 1 and 2 respectively. Results of the Raman spectral analysis is reported in Table 1. The figures clearly show two spectral features centred upon 1008 and 840 cm^{-1}representing the SO_4^{2-} and UO_2 symmetric stretching regions. A single band is observed at around 1008.7 cm^{-1} in the 298 K spectrum and at 1008.9 cm^{-1} in the 77 K spectrum and is assigned to the SO_4^{2-} symmetric stretching vibration. The band shows a slight shift to higher wavenumbers upon cooling to 77 K. Variation in both intensity and band position in the spectral profiles especially for the spectrum of the UO_2^{2+} occurs depending on the sample origin. Variation in the peak position of the SO_4^{2-} stretching vibrations occurs showing the spectra are sample dependent. Variation in the spectral profile of the UO_2 units also occurs. Three bands are observed at around 842.5, 834.7 and 818 cm^{-1}. This variation becomes more pronounced in the 77 K spectra. Improved band separation occurs at 77 K. For the spectrum of the sample from the Ranger deposit, three bands are resolved at 844.5, 834.5 and 820.0 cm^{-1}. It is clear that the Raman spectra of the uranopilite are sample dependent. Variations in peak positions are only slight in the case of bands attributed to the $(SO_4)^{2-}$ vibrations since all sulfate oxygens are located in the equatorial plane of uranyls. Greater shifts are observed in peak positions of bands connected with the $(UO_2)^{2+}$ stretching vibrations. The reason for it is that uranyl oxygens participate in the formation and arrangement of hydrogen-bond network. The arrangement of hydrogen-bond network may vary in the uranopilite samples of the same and especially different localities.

The infrared spectra of the four uranopilite minerals in the 550 to 1250 cm^{-1} region are displayed in Figure 3. These spectra show a complex set of overlapping

bands which makes the identification of a single band or component band to symmetric stretching vibrations difficult. In the infrared spectrum a low intensity band is observed at around 1005 cm^{-1} and is assigned to this SO_4^{2-} symmetric vibration. The Raman spectra in the 1050 to 1350 cm^{-1} region of the uranopilite at 298 and 77 K are shown in Figures 4 and 5. Four bands are observed at around 1178, 1145, 1115 and 1096 cm^{-1} for each of the uranopilite minerals. These bands are ascribed the SO_4^{2-} antisymmetric stretching vibrations. A broad band is also observed at 1272 cm^{-1}. It is not known what the attribution of this band is due to, but one possibility is that it is assignable to U-OH deformation modes.

There are four bands observed in the spectral profile centred upon 840 cm^{-1} at 842, 837, 826 and 824 cm^{-1}. These bands are assigned to the UO_2 symmetric stretching vibrations. The bands show a slight shift to higher wavenumbers upon collecting the spectra at 77 K. There are six structurally distinct uranyls in the crystal structure of uranopilite. [40]Six bands related to the ν_3 UO_2^{2+} (infrared spectrum) and the ν_1 UO_2^{2+} (Raman spectrum) may be but need not be observed. [41] The number of expected bands is usually lower. In the infrared spectrum a band is observed at 838.5 cm^{-1} for the South Alligator mineral, 838 cm^{-1} for the ranger mineral, 830 and 821 cm^{-1} for the Apex mine sample 828 cm^{-1} for the Midnight Mine sample. These bands are the infrared activated symmetric stretching modes. A set of bands is observed in the infrared spectrum which is not observed in the Raman spectra in the 900 cm^{-1} region (Figure 5). The spectral profile in the 850 to 950 cm^{-1} region is complex with multiple overlapping bands. Infrared bands are observed at 932, 912, 888 and 863 cm^{-1} for the South Alligator River sample; 941, 929, 910 and 884 cm^{-1} for the ranger mineral; 925, 905 and 891 cm^{-1} for the Apex Mine sample; 941, 929 and 900 cm^{-1} for the Midnite mine sample. The probable assignment of these bands is to the ν_3 antisymmetric stretching modes of the UO_2 units, although there may be also a coincidence of the uranyl stretching vibrations bands and those of δ U-OH bending bands.

The Raman spectra in the low wavenumber region are shown in Figure 6. Intense bands are observed at 559 and 546 cm^{-1} for the South alligator mineral sample. Bands are observed in similar positions for the other minerals. These bands are attributed to the ν_4 bending modes of the $(SO_4)^{2-}$ units. The observation of more than one band in this spectral region suggests a lowering of the symmetry of the sulphate anion from to C_{3v} or less. Bands in the 407 cm^{-1} region are assigned to the ν_2 SO_4^{2-} bending vibrations. Some bands may be also related to the ν U-$O_{equatorial}$, i.e. U-O_{ligand} vibrations [42]. A band is observed at 407 cm^{-1} at 298 K for each of the minerals and 412 cm^{-1} at 77 K and is attributed to the ν_2 bending mode of the $(SO_4)^{2-}$ units. Intense bands observed in the Raman spectra at 77 K are also connected with these ν_2 SO_4^{2-} bending vibrations. Bands at wavenumbers lower than 320 cm^{-1} observed in the Raman spectra (Fig. 6) - not measured in the infrared spectra, are attributed to the ν_2 (δ) UO_2^{2+} bending vibrations and the lowest bands (180-211 cm^{-1}) may be assigned to the lattice and/or O_l-U-O_{ligand} vibrations [43] and /or cation and anion librations [44]. In each of the spectra bands are observed at around 322, 294, 260 cm^{-1}. Any unambiguous assignment of bands in this range is very complex.

Because of the complex infrared spectral profile in the region of the ν OH stretching vibrations [Frost et al. 2005 [32]and this paper] which is related to the

complex crystal structure of uranopilite, some assignments of the Raman and infrared spectra from the papers by Dothee [45,46] offering more detailed band interpretation may be applied. Some coincidences of the bands of the $(UO_2)^{2+}$ stretching vibrations and those of δU-OH and/or γU-OH bending vibrations may be expected. With respect to the above described tentative assignment of infrared and Raman bands of uranopilite samples studied, it is shown below that some assignment may be given in more structural detail. Thus some bands observed close to 700 cm^{-1} may be attributed to the libration modes of crystal water, while those in the range 600-700 cm^{-1} to libration modes of coordination water. Bands in the range 800-920 cm^{-1} and 600-800 cm^{-1} may be assigned to the δU-OH and γU-OH bending vibrations, respectively. Bands at lower wavenumbers than 600 cm^{-1} may be also interpreted as connected with the ν (U_3O) bridge elongation (approximately at 550- 450 cm^{-1}), $U_2O(OH)$ bridge elongation (360-380 cm^{-1}), ν $U_3(OH)_3$ group elongation and γ (U_3O) out-of plane bending (340-320 cm^{-1}), δ $(UO_2)^{2+}$ (<300- 240 cm^{-1}), γ ($U_3(OH)_3$) out-of-plane bending and δ ($U_3(OH)_3$) in-plane bending (close to 210 cm^{-1}) [for further details see e.g.Dothée and Camelot 1982; Dothée et al. 1982; Čejka 1999] [30,45,46]. All the mentioned structural units may be observed in the crystal structure of uranopilite.

Empirical relations $R_{U-O} = f(\nu_1 \text{ or } \nu_3 (UO_2)^{2+})$ enable the calculation of U-O bond lengths in uranyl compounds. In this paper the relations by Bartlett and Cooney [47] are used . Calculated lengths are compared with thou of the crystal structure analysis of uranopilite [40].

Infrared spectra/ Raman spectra 298/Raman 77K (R_{U-O} Å/ν_3 or ν_1 $(UO_2)^{2+}$ cm^{-1}) in uranopilite samples studied [after Bartlett and Cooney 1989]

South Alligator River

IR ν_3 $(UO_2)^{2+}$ 1.762/932.2; 1.775/912.7; 1.793/888.7/; 1.812/863.4
IR ν_1 $(UO_2)^{2+}$ 1.7495/863.4 ; 1.773/838.5; 1.823/788
Raman 298K ν_3 $(UO_2)^{2+}$ 1.796/884.2; 1.804/874.4
Raman 298 K ν_1 $(UO_2)^{2+}$ 1.769/842.4; 1.774/837.3; 1.784/826.3; 1.786/824.6; 1.807/803.7

Ranger No.1 Deposit

IR ν_3 $(UO_2)^{2+}$ 1.756/941.4; 1.764/929.1; 1.777/910.1; 1.796/884.3
IRν_1 $(UO_2)^{2+}$ 1.773/838; 1.803/807.4
Raman 298K ν_3 $(UO_2)^{2+}$ 1.782/903
Raman 298K ν_1 $(UO_2)^{2+}$ 1.768/843.6; 1.770/841.4; 1.774/836.9; 1.792/818.7
Raman 77K ν_3 $(UO_2)^{2+}$ 1.794/886.6; 1.819/854.2
Raman 77K ν_1 $(UO_2)^{2+}$ 1.758/854.2 (?); 1.767/844.6; 1.776/834.6; 1.791/820

Apex Mine

IR ν_3 $(UO_2)^{2+}$ 1.767/925.3; 1.781/905.1; 1.791/891.8
IR ν_1 $(UO_2)^{2+}$ 1.780/830.4; 1.790/820.9; 1.812/798.5
Raman 298K ν_3 $(UO_2)^{2+}$ 1.785/899.8

Raman 298K ν_1 $(UO_2)^{2+}$ 1.768/843.4; 1.771/840.5; 1.775/836.6; 1.792819.1
Raman 77k ν_1 $(UO_2)^{2+}$ 1.768/843.9; 1.769/842; 1.777/834.1; 1.791/820.1

Midnite Mine

IR ν_3 $(UO_2)^{2+}$ 1.756/941; 1.764/929.3; 1.784/900.6; 1.810/866.5
IR ν_1 $(UO_2)^{2+}$ 1.747/866.5 (?); 11.770/841.1; 1.783/828.2; 1.819/791.8
Raman 298K ν_1 $(UO_2)^{2+}$ 1.769/842.5; 1.773/838.6; 1.776/834.7; 1.792/818.1
Raman 77K ν_1 $(UO_2)^{2+}$ 1.766/845.1; 1.769/842.3; 1.778/833.3; 1.785/825.5; 1.794/816.3.

Average U-O bond lengths in uranopilite inferred from the X-ray single crystal structure analysis by Burns [40] is 1.79 Å, average U-O bond lengths for six symmetrically distinct uranyls are 1.81, 1.82, 1.80, 1.79, 1.76 and 1.76 Å. The U-O bond lengths vary in the range 1.72(2) – 1.87(2) Å. U-O bond lengths in uranyls inferred from the Raman and infrared spectra are in good agreement and comparable with those from the X-ray single crystal structure analysis. [40] However, some differences between the uranopilite samples studied are observed. This proves that the crystal structures of the uranopilite studied are very similar but not exactly identical. It is assumed that the main role influencing the differences is the arrangement of the hydrogen-bonding network in the structures. This manuscript goes a long way in explaining these structures.

Hawthorne [19,21] writes that hydrogen plays an extremely important role in the structure and chemistry of the oxide and oxysalt minerals. Water molecules and other O-H groupings such as hydroxyls and hydrogen bonding are of fundamental importance to the stability of the structure of most uranyl minerals inclusive uranopilite [15]. Many papers discussing thermal stability of hydrated minerals (e. g. some uranyl silicates or uranyl phosphates) have assumed that a part of water molecules may be classified as zeolitic water [3,48]. Hawthorne proves that such assumptions are incorrect. Uranopilite dehydrates in several steps [28,49-51] [10,11,28,49-51]. An intermediate the composition of which corresponds to meta-uranopilite is in fact X-ray amorphous. Burns proposed a model for hydrogen bonding in uranopilite. Water molecules and hydroxyls present in the uranyl sulfate chains together with interstitial water molecules participate in the formed hydrogen bonding network. It was proved that structures of uranyl sulfate minerals are not stable and may be destroyed e.g. by sample preparation for X-ray and/or even vibrational spectral measurements.

Infrared spectra of uranopilite in the 2500 to 3700 cm^{-1} range are given in the Figure 7. The observed bands attributed to ν OH stretching vibrations prove a complex arrangement of OH groupings i.e. water molecules and OH^- ions, and hydrogen bonding in the crystal structure of uranopilite. There are structurally distinct water molecules (this is proved also by δ H_2O bending vibrations observed in the 1575 – 1670 cm^{-1} Figure 8) and hydroxyls. The presence of strong and weak O-H…O hydrogen bonds were inferred from these observations [52]. Because of this "dependence" on actual arrangement of hydrogen bonding network, Raman and infrared spectra of uranopilite samples from various localities and origin may differ.

O-H…O bond lengths (Å) vs infrared ν OH stretching vibrations in the structure of uranopilite samples studied [after Libowitzky 1999] [52]

South Alligator River	Ranger No.1 Deposit	Apex Mine	Midnite Mine
			>3.2/3964.7
		>3.2/3600.3	>3.2/3622.5
	3.09/3569.8	3.05/3561.5	>3.2/3587.2
3.03/3555.4			3.0/3549.9
		2.93/3517.5	2.98/3538.3
		2.92/3510.0	
2.87/3470.9	2.89/3490.5		2.87/3470.4
		2.83/3428.5	
	2.8/3397.2		2.79/3392
2.74/3267.7	2.73/3252.7	2.74/3273.7	2.72/3229
2.69/3136.3			
2.67/3064.1	2.68/3073.6	2.66/3027.8	2.67/3048.6
	2.65/2985.5		
2.63/2877.1	2.63/2851.3		
	2.59/2607.7	2.6/2698.2	2.58/2521.8
			2.56/2347.7

Infrared bands in the 1398 to 1442 cm^{-1} and Raman bands close to 1380 cm^{-1} may be probably tentatively attributed to the δ U-OH bending (deformation) vibrations and/or overtones and/or combination bands, Raman bands close to 1900 cm^{-1} to overtones or combination bands.

4. Conclusions

Uranopilite is one of the minerals the stoichiometric composition of which may vary to some extent. This is connected especially with spontaneous partial dehydration of uranopilite. Because of hydrolytical processes proceeding in nature, hydrolysis of uranopilite connected with the partial lowering of sulfate ion contents cannot be also excluded. This indicates that intermediates in the series uranopilite-schoepite may be observed. Water molecules and hydroxyls present in the uranyl sulfate chains together with interstitial water molecules participate in the formed hydrogen bonding network. Some variability in the νOH stretching vibrations proves that the structure of uranopilite originating from different localities may also vary to some extent.

Raman spectroscopy at 298 and 77 K together with infrared spectroscopy has been used to assist in the elucidation of the uranopilite mineral structure. Bands connected with $(UO_2)^{2+}$ and $(SO_4)^{2-}$ vibrations, U-OH vibrations, and water and hydroxyl vibrations are observed and attributed. U-O bond lengths in uranyls and O-H…O bond lengths were calculated and proved that uranopilite studies are structurally comparable but not exactly identical. Possible assignments of bands to the (U_3O), $U_3(OH)_3$ and $U_2O(OH)$ vibrations were also mentioned.

Conclusions related to the hydrogen-bonding network in uranopilite studied support the Hawthorne hypothesis that the weak interaction between the structural unit, i.e. the uranyl sulfate chains, and the interstitial complex, i.e. interstitial water molecules, controls the stability of the structural arrangement. [53]

Acknowledgements

The financial and infra-structure support of the Queensland University of Technology Inorganic Materials Research Program of the School of Physical and Chemical Sciences is gratefully acknowledged. The Australian Research Council (ARC) is thanked for funding. Mr Dermot Henry of Museum Victoria is thanked for the supply of the selected uranopilite minerals. Comments by Nicolas Meisser on this manuscript to the authors are greatly appreciated.

References

1. Brugger, J, Wallwork, KS, Meisser, N, Pring, A, Ondrus, P, Cejka, J. *American Mineralogist* 2006**; 91**: 929.
2. Brugger, J, Burns, PC, Meisser, N. *American Mineralogist* 2003**; 88**: 676.
3. Frondel, C, Weeks, AD. *Proc. UN Intern. Conf. Peaceful Uses Atomic Energy, 2nd, Geneva,* 1958**; 2**: 277.
4. Frondel, C. *U.S. Geological Survey Bulletin* 1958**; No. 1064**: 400 pp.
5. Novácek, R. Věstnik Kral. České Spol. Nauk 1935: 35.
6. Anthony, JW, Bideaux, RA, Bladh, KW, Nichols, MC *Handbook of Mineralogy*; Mineral Data Publishing: Tiscon, Arizona, USA, 2003; Vol. 5.
7. Novacek, R. *Vestnik Kral. Ceske Spol. Nauk* 1942: 13 pp.
8. Frondel, C. *American Mineralogist* 1952**; 37**: 950.
9. Novacek, R. *Vestnik Kral. Ceske Spol. Nauk* 1935**; Cl. 2**: 36 pp.
10. Ondrus, P, Veselovsky, F, Hlousek, J. *Journal of the Czech Geological Society* 1997**; 42**: 109.
11. Ondrus, P, Veselovsky, F, Skala, R, Cisarova, I, Hlousek, J, Fryda, J, Vavrin, I, Cejka, J, Gabasova, A. *Journal of the Czech Geological Society* 1997**; 42**: 77.
12. Ondrus, P, Skala, R, Veselovsky, F, Sejkora, J, Vitti, C. *American Mineralogist* 2003**; 88**: 686.
13. Jensen, KA, Palenik, CS, Ewing, RC. *Radiochimica Acta* 2002**; 90**: 761.
14. Jensen, KA, Janeczek, J, Ewing, RC, Stille, P, Gauthier-Lafaye, F, Salah, S. *Materials Research Society Symposium Proceedings* 2000**; 608**: 525.
15. Jensen, KA, Ewing, RC, Gauthier-Lafaye, F. *Materials Research Society Symposium Proceedings* 1997**; 465**: 1209.
16. Meisser, N, Brugger, J, Lahaye, Y. *B. Kríbek & J. Zeman, eds.* 2000: 147.
17. Burns, PC. *Materials Research Society Symposium Proceedings* 2004**; 802**: 89.
18. Burns, PC, Miller, ML, Ewing, RC. *Canadian Mineralogist* 1996**; 34**: 845.
19. Hawthorne, FC. *Zeitschrift fuer Kristallographie* 1992**; 201**: 183.
20. Hawthorne, FC. *Acta Crystallographica, Section B: Structural Science* 1994**; B50**: 481.
21. Hawthorne, FC. *EMU Notes in Mineralogy 1* 1997**; European Mineralogical Union**: 373.
22. Cejka, J, Sejkora, J, Mrazek, Z, Urbanec, Z, Jarchovsky, T. *Neues Jahrbuch fuer Mineralogie, Abhandlungen* 1996**; 170**: 155.
23. Finch, RJ, Cooper, MA, Hawthorne, FC, Ewing, RC. *Canadian Mineralogist* 1996**; 34**: 1071.
24. Finch, RJ, Hawthorne, FC, Ewing, RC. *Materials Research Society Symposium Proceedings* 1996**; 412**: 361.
25. Finch, RJ, Hawthorne, FC. *Canadian Mineralogist* 1998**; 36**: 831.
26. Omori, K, Kerr, PF. *Geological Society of America Bulletin* 1963**; 74**: 709.
27. Frost, RL, Carmody, O, Erickson, KL, Weier, ML, Henry, DO, Cejka, J. *Journal of Molecular Structure* 2004**; 733**: 203.
28. Cejka, J, Urbanec, Z. *Zb. Celostatnej Konf. Term. Anal., 8th* 1979: 177.
29. Cejka, J, Sejkora, J, Deliens, M. *Neues Jahrbuch fuer Mineralogie, Monatshefte* 1996: 125.
30. Cejka, J. *Reviews in Mineralogy* 1999**; 38**: 521.

31. Frost, RL, Weier, ML, Martens, W, Cejka, J. *Vibrational Spectroscopy* 2006**; 41**: 205.
32. Frost, RL, Erickson, KL, Cejka, J, Reddy, BJ. *Spectrochimica Acta, Part A: Molecular and Biomolecular Spectroscopy* 2005**; 61**: 2702.
33. Frost, RL, Weier, ML, Bostrom, T, Cejka, J, Martens, W. *Neues Jahrbuch fuer Mineralogie, Abhandlungen* 2005**; 181**: 271.
34. Cejka, J, Urbanec, Z, Cejka, J, Jr., Mrazek, Z. *Neues Jahrbuch fuer Mineralogie, Abhandlungen* 1988**; 159**: 297.
35. Jensen, KA, Palenik, CS, Burns, PC, Ewing, RC. *Abstracts of Papers, 222nd ACS National Meeting, Chicago, IL, United States, August 26-30, 2001*: NUCL.
36. Frost, RL, Weier, ML. *Thermochimica Acta* 2003**; 406**: 221.
37. Frost, RL, Weier, ML, Kloprogge, JT. *Journal of Raman Spectroscopy* 2003**; 34**: 760.
38. Frost, RL, Weier, ML. *Journal of Raman Spectroscopy* 2003**; 34**: 776.
39. Frost, RL, Weier, ML. *Thermochimica Acta* 2004**; 409**: 79.
40. Burns, PC. *Canadian Mineralogist* 2001**; 39**: 1139.
41. Serezhkina, LB, Serezhkin, VN, M. A. Soldatkina. *Zh. Neorg. Khim.* 1982**; 27**: 1750.
42. Hoekstra, HR, Siegel, S. *Journal of Inorganic and Nuclear Chemistry* 1973**; 35**: 761.
43. Volod'ko, LV, Komyak, AI, Umreiko, DS *Uranyl Compounds, Vol. 1: Spectra, Structure*, 1981.
44. Anderson, A, Chieh, C, Irish, DE, Tong, JPK. *Canadian Journal of Chemistry* 1980**; 58**: 1651.
45. Dothee, DG, Fahys, BR, Camelot, MM. *Bulletin de la Societe Chimique de France* 1982: 103.
46. Dothee, DG, Camelot, MM. *Bulletin de la Societe Chimique de France* 1982: 97.
47. Bartlett, JR, Cooney, RP. *Journal of Molecular Structure* 1989**; 193**: 295.
48. Smith, DK. *Institution of Mining and Metallurgy, London* 1984**; B. De Vivo , F. Ippolito, G. Capaldi & P. R. Simpson, eds**: 43.
49. Cejka, J, Urbanec, Z. *Casopis Narodniho Muzea v Praze, Rada Prirodovedna* 1979**; 146**: 114.
50. Ambartsumyan, TL. *Atomnaya Energ., Voprosy Geol. Urana, Suppl.* 1957: 86.
51. Urbanec, Z, Cejka, J. *Therm. Anal., [Proc. Int. Conf. Therm. Anal.], 6th* 1980**; 2**: 359.
52. Libowitzky, E. *Monatshefte fuer Chemie* 1999**; 130**: 1047.
53. Hawthorne, FC. *Geologiya Rudnykh Mestorozhdenii* 2003**; 45**: 100.

ATR-IR				298K Raman				77K Raman		
South Alligator River	Ranger No. 1 Deposit	Apex Mine	Midnite Mine	South Alligator River	Ranger No. 1 Deposit	Apex Mine	Midnite Mine	Ranger No. 1 Deposit	Apex Mine	Midnite Mine
			3694.7							
		3600.3	3622.5							
	3569.8	3561.5	3587.8							
3555.4			3549.9							
		3517.5	3538.3							
		3510.0								
3470.9	3490.5		3470.4							
3418.5		3428.5								
	3397.2		3392.0							
3267.7	3252.7	3273.7	3229.9							
3136.3										
3064.1	3073.6	3027.8	3048.6							
	2985.5									
2877.1	2851.3									
	2607.8	2698.2	2521.8							
			2347.7							
				1906.8	1904.3	1905.3	1904.9		1905.2	1905.4
1663.8										
1625.0	1625.3	1622.8	1627.5							
1575.0		1618.2	1619.2							
1558.6										
1539.9	1534.3	1534.9	1546.9							
1526.0										
1511.4										
1421.1	1420.8	1442.5	1418.2							
1398.6							1380.4		1380.9	

				1272.2	1267.9	1272.0	1272.2		1271.2	1267.4
	1159.4	1169.6		1178.5	1177.3	1176.7	1179.2		1178.1	1170.2
1137.8	1141.1	1137.6	1140.8	1145.0	1141.3	1141.4	1141.9	1148.1	1147.4	1147.4
								1130.2		
1118.2	1118.2	1113.5	1116.5	1115.1	1114.4	1114.4	1114.3	1118.4	1115.7	1113.5
1100.4	1099.0	1097.2	1102.4	1096.1	1095.9	1095.4	1095.2	1105.9	1094.9	1095.3
	1072.4	1070.4	1095.8							
1031.8		1037.5	1031.9							
	1005.7	1008.8	1009.7	1009.4	1008.8	1008.7	1008.7	1012.3	1012.2	1010.0
982.1			998.6						1008.9	1008.5
932.2	941.3		941.0							
	929.1	925.3	929.3							
912.7	910.1	905.1	900.6		903.0	899.8				
888.7	884.3	891.8		884.2				886.6		
863.4			866.5	874.3				854.2		
838.5	838.0		841.1	842.4	843.6	843.4	842.5	844.6	843.9	845.1
					841.4	840.5	838.6	834.6	842.0	842.3
		830.4	828.2	837.3	836.9	836.6	834.7	820.0	834.1	833.3
		820.9		826.3	818.7	819.1	818.1		820.1	825.5
				824.6						816.3
788.0	807.4	798.5	791.8	803.7						
			759.0							
740.5		745.8	746.6							
702.6			687.1							
		674.1	662.2	664.3	663.6	663.7	664.1	666.3	667.5	662.9
			652.8							
602.4	604.7	606.6	609.9	609.0	603.6	559.6	558.5	604.8	602.9	
		580.0	602.1						571.5	
		560.2	554.6	559.5	559.3			563.5	567.1	552.7
		549.8	542.4	546.0	546.1	546.1	544.4	549.9	550.9	543.8
		543.5								

		535.6								
		535.2	534.1						513.3	
				456.6	477.3	475.2	476.5	478.7	479.1	480.5
				437.1						
				407.7	407.4	407.1	407.3	412.9	409.1	412.4
									375.0	381.1
										341.5
				332.8	323.6	322.2	323.9	321.2	325.5	325.1
				321.7						302.6
				294.6	298.0	296.2	294.2	295.5	298.3	295.0
				260.1	259.7	259.7			256.9	266.1
					252.9	255.4	258.5	252.6		256.5
							246.3			247.2
								239.0		236.2
				224.9		225.4	231.3	228.4	229.5	231.3
				207.6		203.7	212.0	210.9	202.5	210.5
				195.8		194.6	194.8		196.5	196.8

Table 1. Results of the spectroscopic analysis of the band centres of the infrared spectra and the Raman spectra of uranopilite from (a) Ranger No. 1 deposit, Jabiru, NT (b) South Alligator River, NT (c) Apex Mine, Lander Co., Nevada (d) Midnite Mine, Stevens Co., Washington.

List of Figures

List of Tables

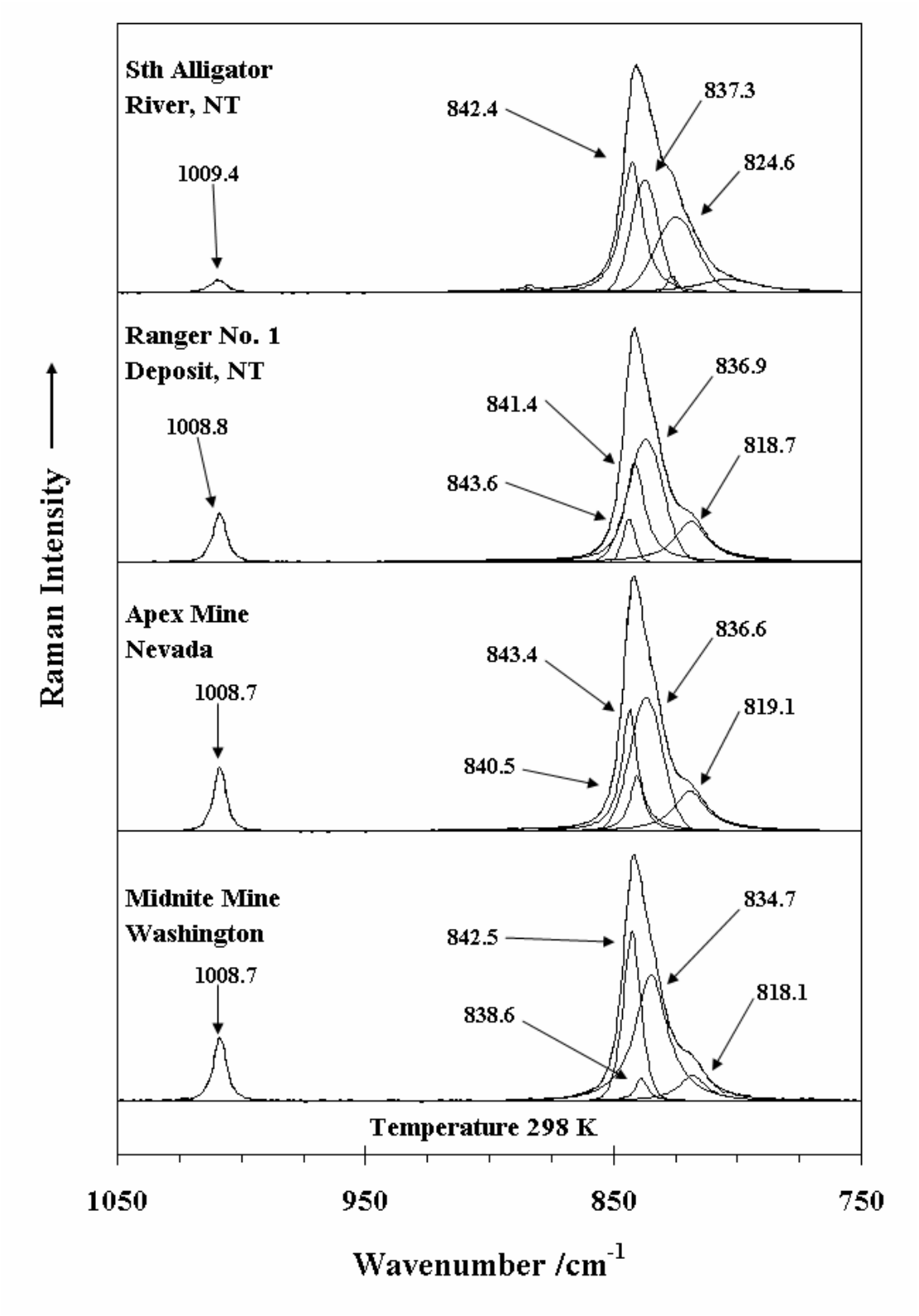
Sth Alligator
River, NT
1009.4
842.4
837.3
824.6
Ranger No. 1
Deposit, NT
1008.8
841.4
843.6
836.9
818.7
Apex Mine
Nevada
1008.7
843.4
840.5
836.6
819.1
Midnite Mine
Washington
1008.7
842.5
838.6
834.7
818.1
Raman Intensity
Temperature 298 K
1050
950
850
750
Wavenumber /cm-1

Figure 1

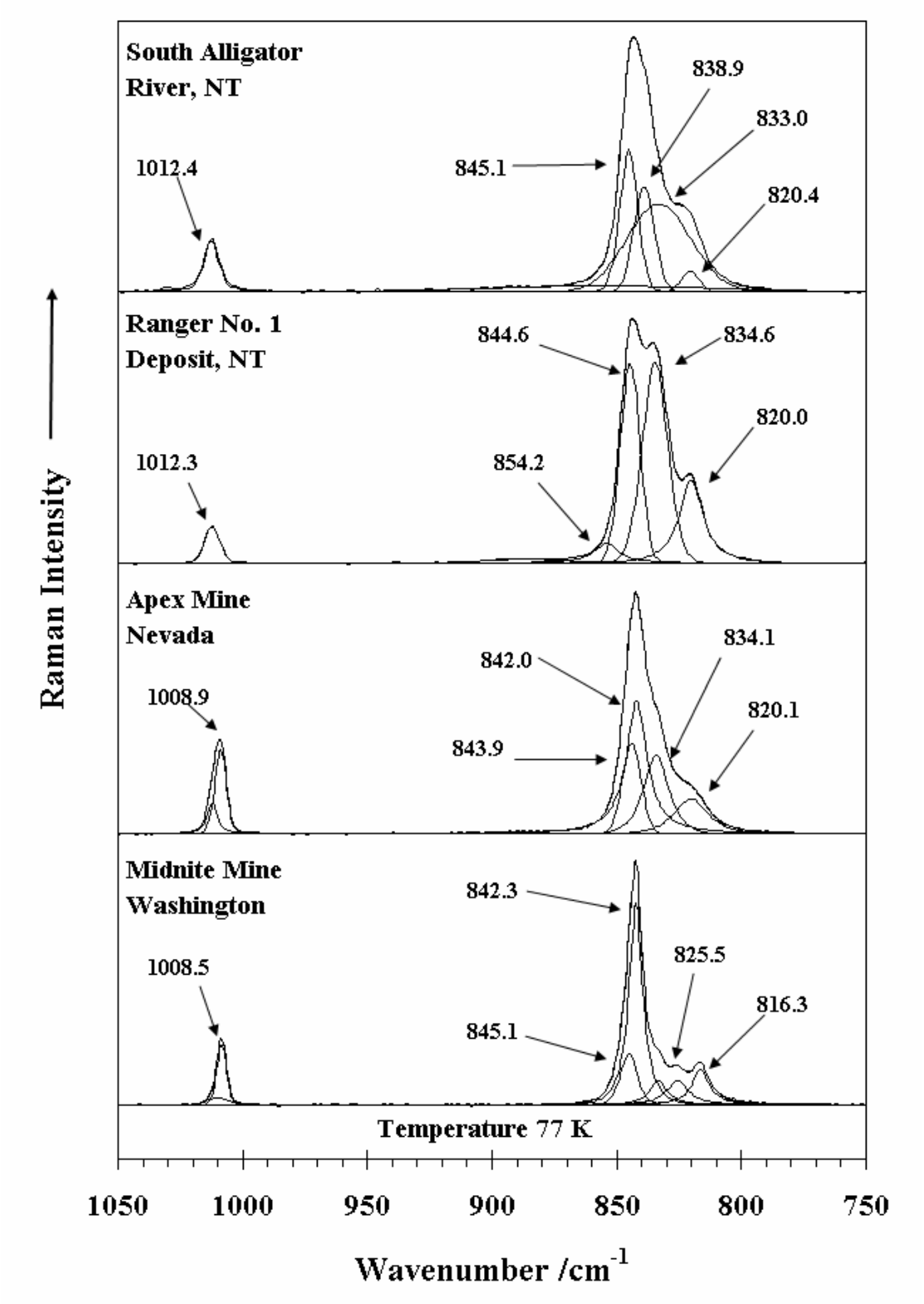
South Alligator
River, NT
1012.4
845.1
838.9
833.0
820.4
Ranger No. 1
Deposit, NT
1012.3
844.6
854.2
834.6
820.0
Apex Mine
Nevada
1008.9
842.0
843.9
834.1
820.1
Midnite Mine
Washington
1008.5
842.3
845.1
825.5
816.3
Raman Intensity
Temperature 77 K
1050
1000
950
900
850
800
750
Wavenumber /cm-1

Figure 2

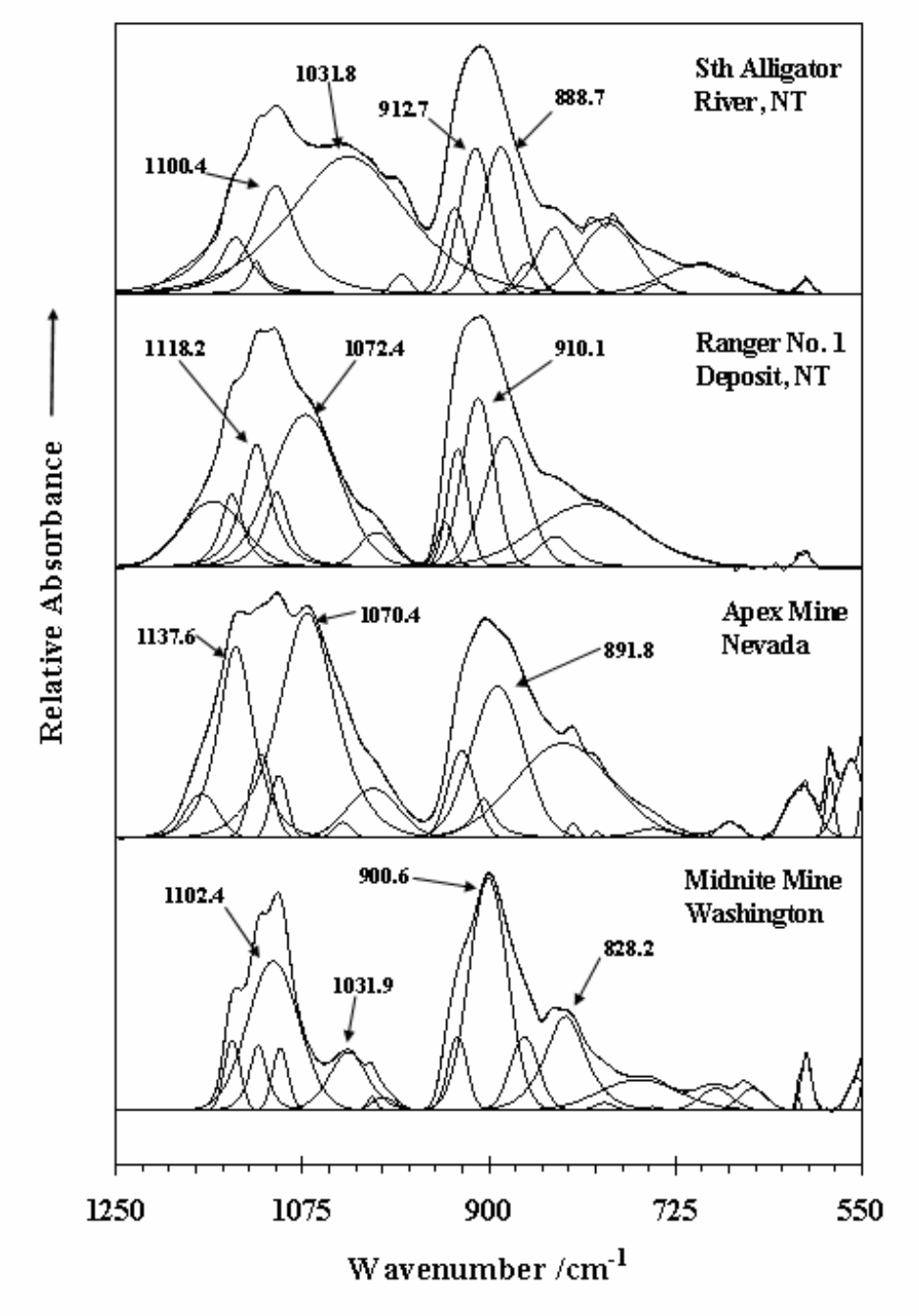
Sth Alligator River, NT
1031.8
912.7
888.7
1100.4
Ranger No. 1 Deposit, NT
1118.2
1072.4
910.1
Apex Mine Nevada
1137.6
1070.4
891.8
Midnite Mine Washington
1102.4
900.6
828.2
1031.9
Relative Absorbance
1250
1075
900
725
550
Wavenumber /cm-1

Figure 3

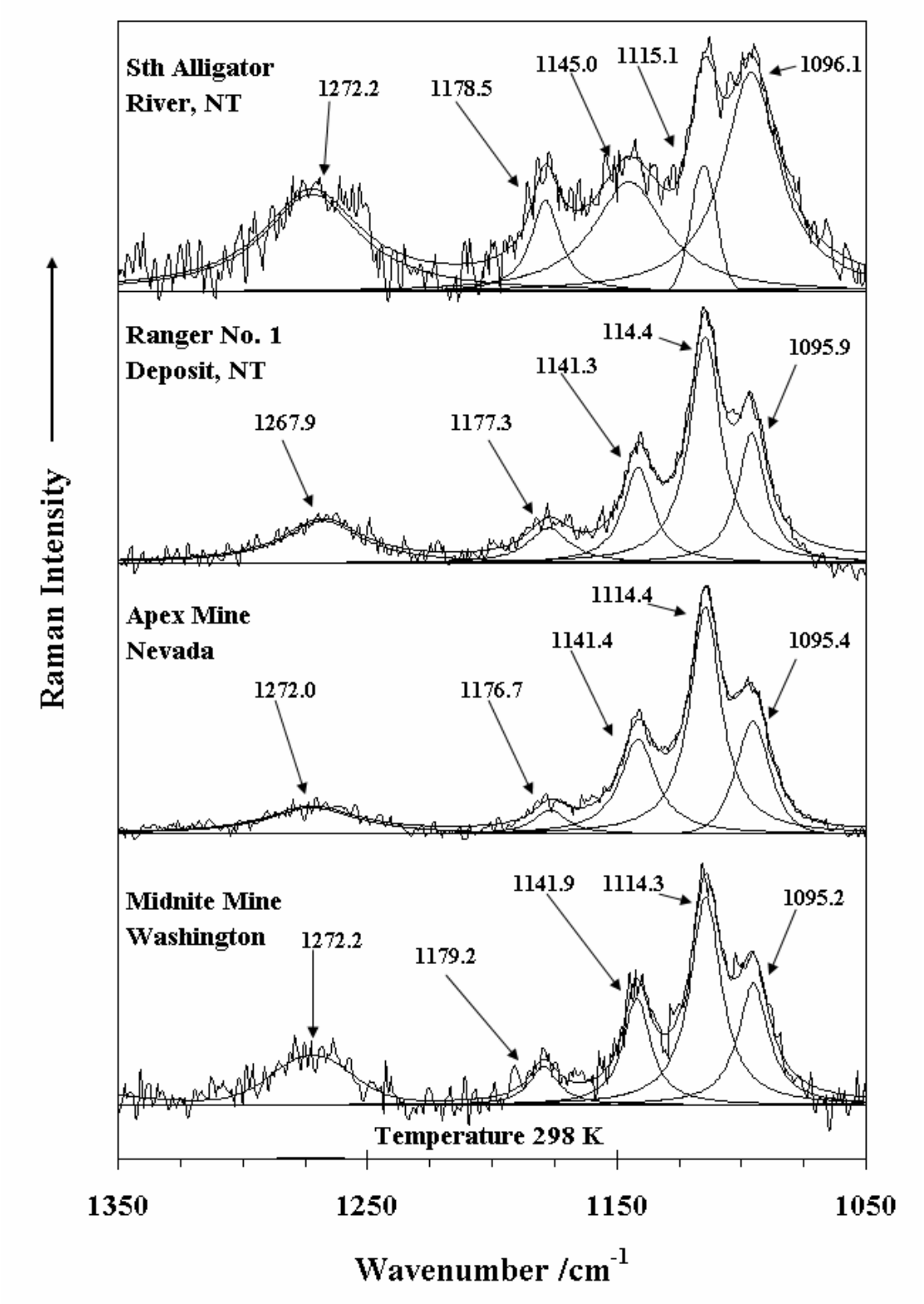

Figure 4 Raman at 298 K

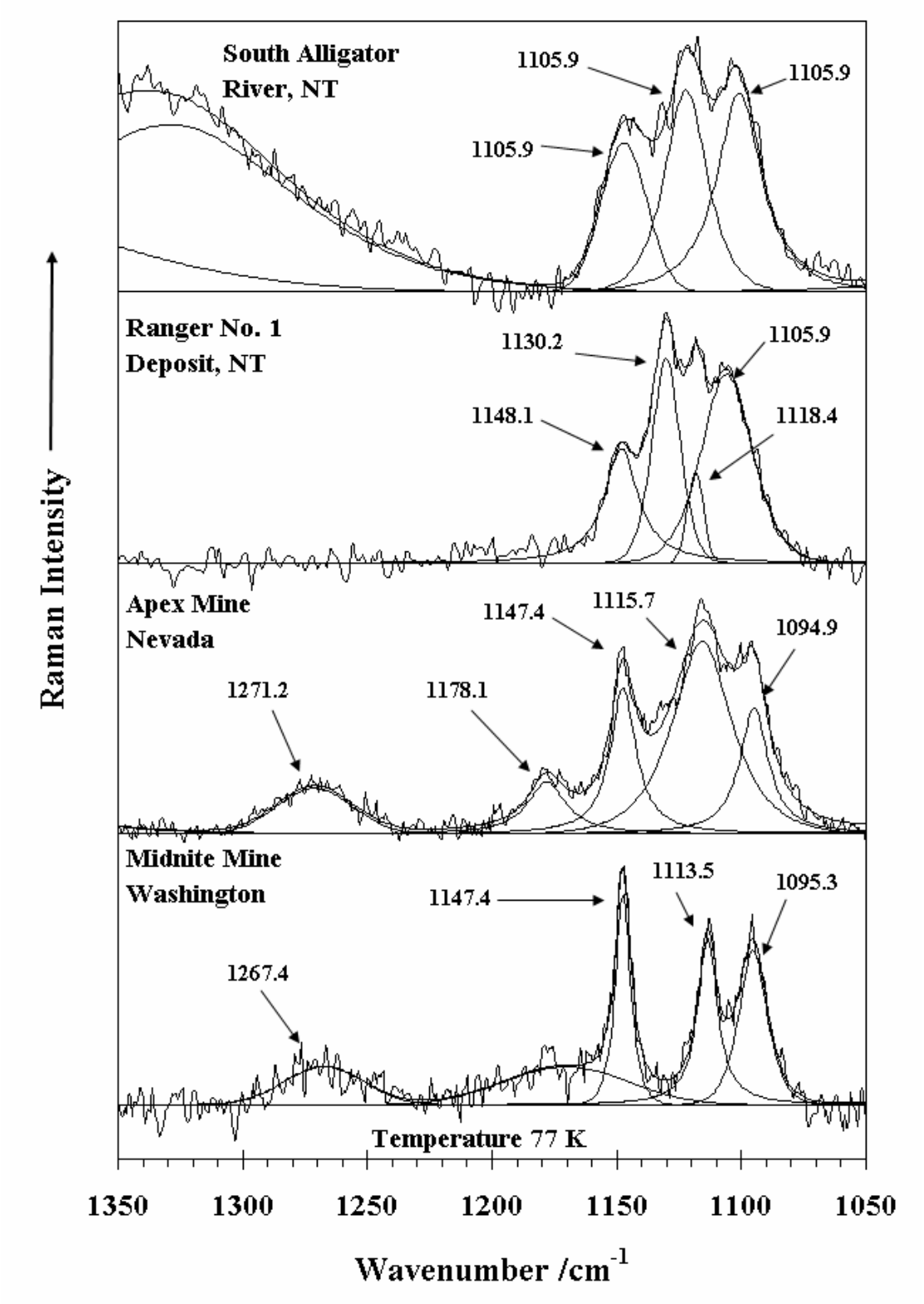

Figure 5 Raman at 77 K

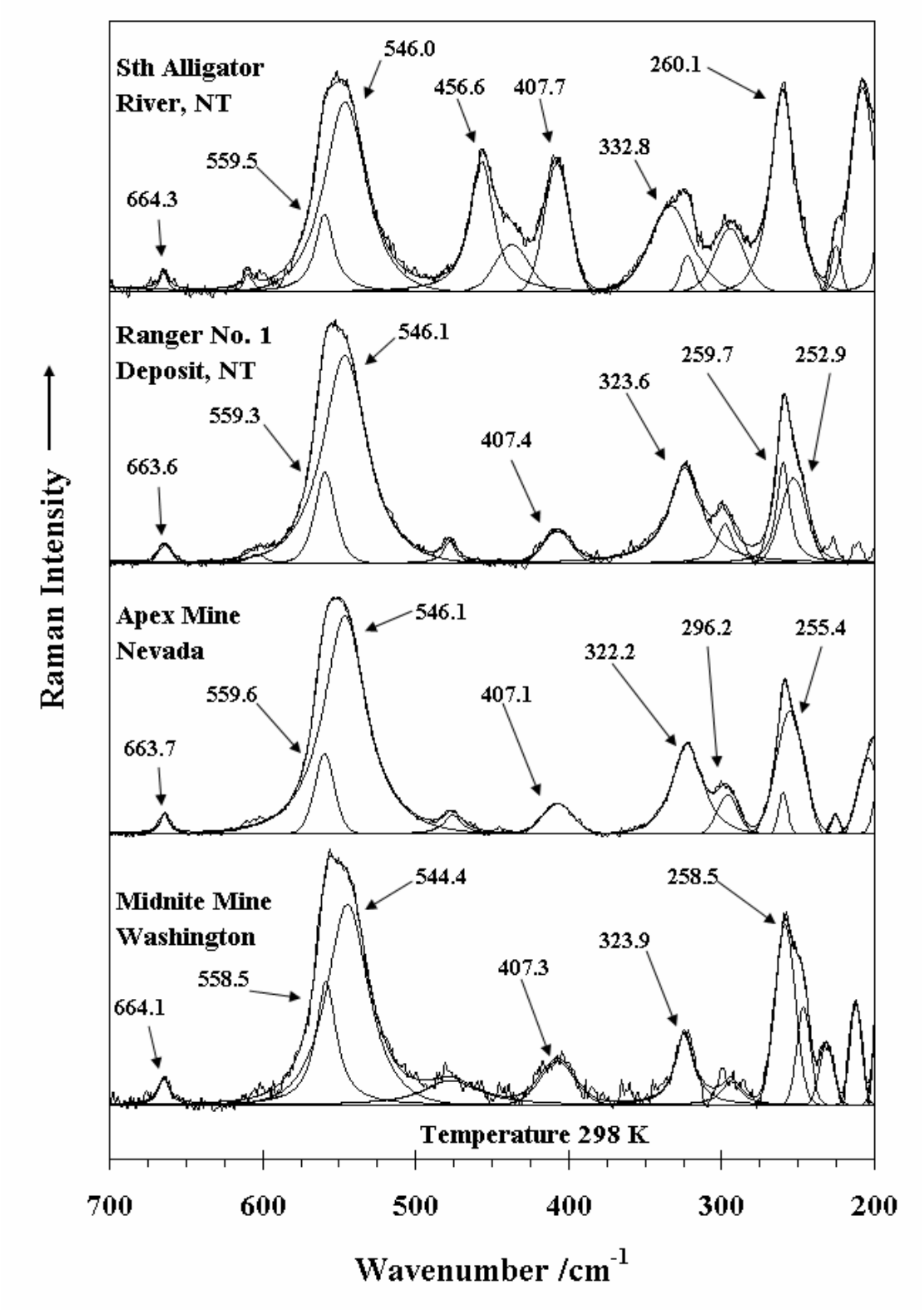

Figure 6 Raman 298 K Low wavenumber region

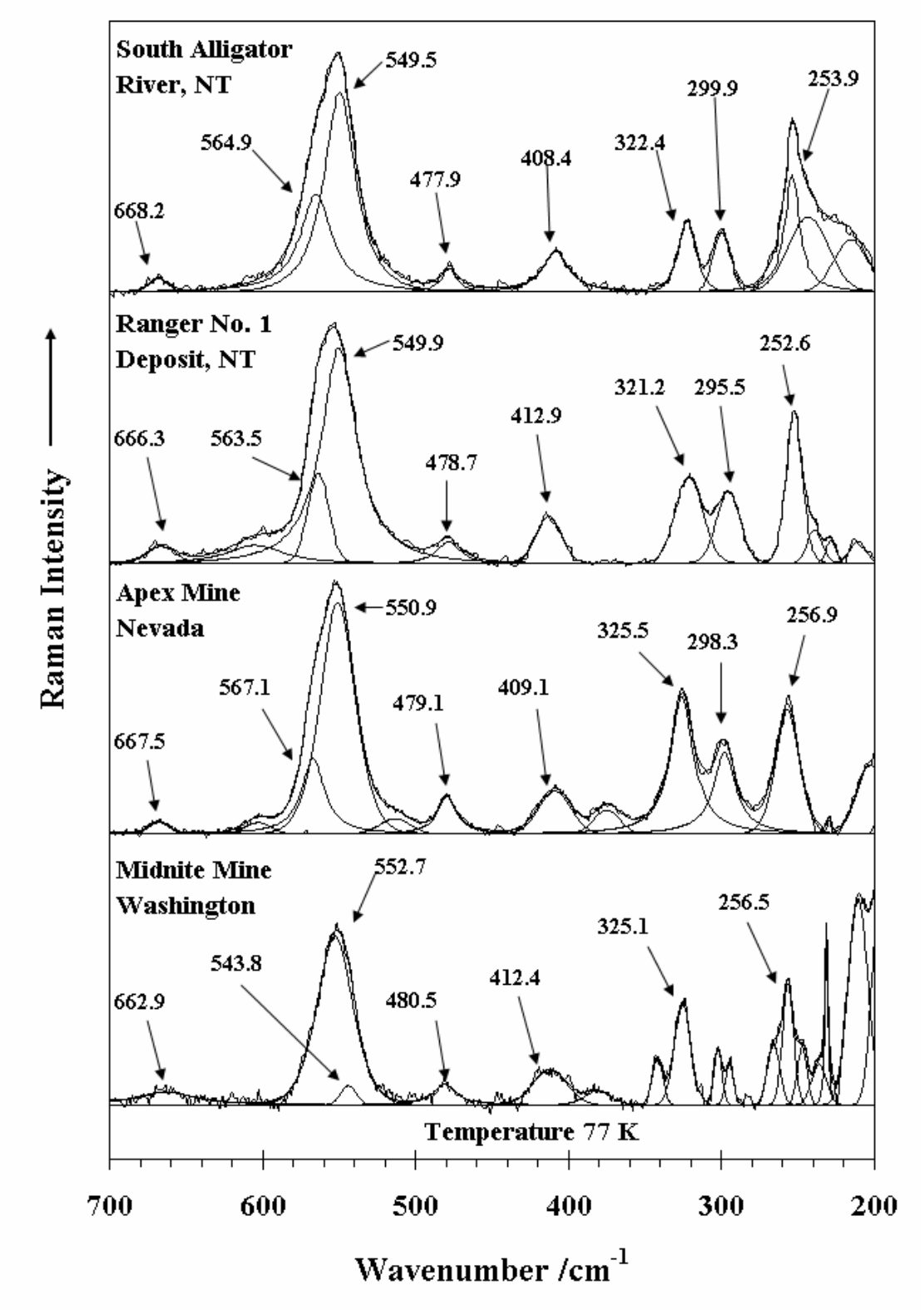

Figure 7 Raman 77 K Low wavenumber region

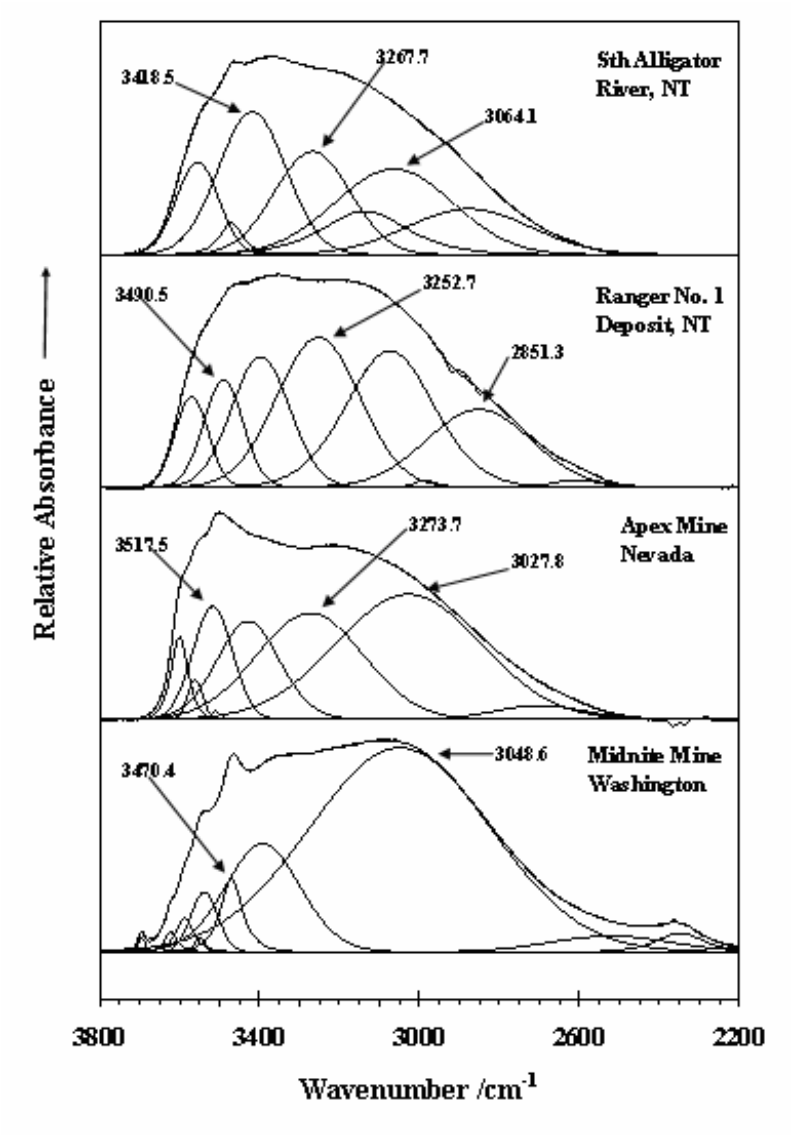

Figure 8 Infrared OH stretching region

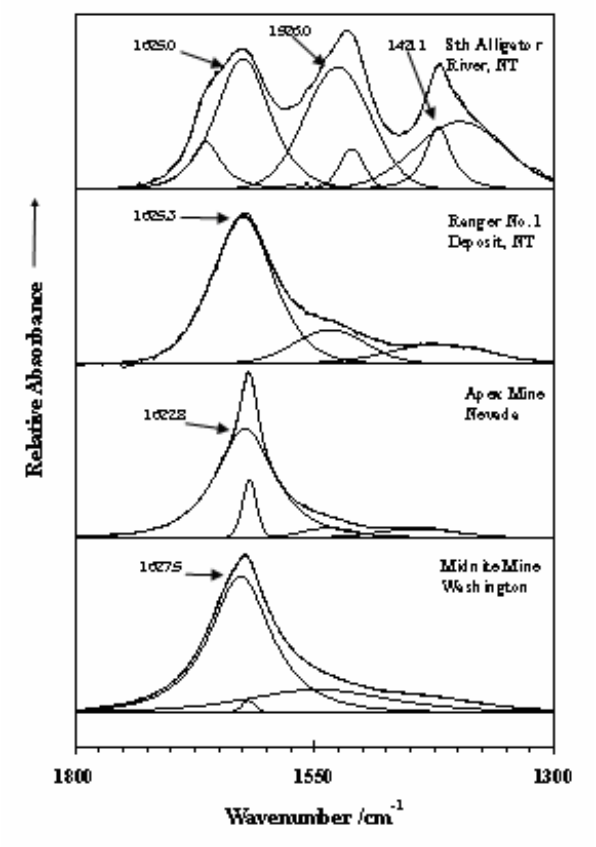

Figure 9 IR OH deformation and HOH bending